Contour Metrology using Critical Dimension Atomic Force Microscopy

Ndubuisi G. Orji, Ronald G. Dixson, András E. Vladár, Bin Ming, Michael T. Postek
Semiconductor and Dimensional Metrology Division
Physical Measurement Laboratory (PML)
National Institute of Standards and Technology, Gaithersburg MD 20899

ABSTRACT

The critical dimension atomic force microscope (CD-AFM), which is used as a reference instrument in lithography metrology, has been proposed as a complementary instrument for contour measurement and verification. Although data from CD-AFM is inherently three dimensional, the planar two-dimensional data required for contour metrology is not easily extracted from the top-down CD-AFM data. This is largely due to the limitations of the CD-AFM method for controlling the tip position and scanning.

We describe scanning techniques and profile extraction methods to obtain contours from CD-AFM data. We also describe how we validated our technique, and explain some of its limitations. Potential sources of error for this approach are described, and a rigorous uncertainty model is presented. Our objective is to show which data acquisition and analysis methods could yield optimum contour information while preserving some of the strengths of CD-AFM metrology. We present comparison of contours extracted using our technique to those obtained from the scanning electron microscope (SEM), and the helium ion microscope (HIM).

Keywords: contour metrology, critical dimension atomic force microscope, scanning electron microscope, helium ion microscope.

1. INTRODUCTION

Contour metrology is one of the techniques used to verify optical proximity correction (OPC) methods in lithography models. The use of OPC methods, which are one type of resolution enhancement technique (RET), are necessitated by the continued decrease in feature sizes. Broadly speaking, OPC methods are used to compensate for lithography errors such as corner rounding caused during image transfer from the mask to the wafer and subsequence processing. This means that proximity effects caused by limitations of the lithography tools are clearly visible after printing. To ensure the intended design are printed, lithographers make use of a series of shapes and assist features that will result in a predictable final printed design. During the lithography process development, the printed features are verified to make sure size and shape requirements are met.

Since some of the limitations of optical lithography are often most difficult near corners and intersections, or other locations lacking translational symmetry, a complete top-down (in plane) contour of the feature gives a better estimate for the models than linewidth at a single location. The contour information once extracted is used to ensure the design is accurately transferred by the lithography tools, and verified by metrology tools. Several studies have highlighted the use of SEMs to measure contours, and specified ways to obtain accurate contour information [1-4]. Other studies have looked at AFM measurement of contours; these include work by Yeon-Ah Shim [5], Ukraintsev [6], and Villarrubia [7]. We have previously presented a preliminary report on this work [8], and it focused on outlining some of the instrumental parameters and uncertainty issues associated with CD-AFM contour metrology.

The critical dimension atomic force microscope (CD-AFM), which is used as a reference instrument in lithography metrology, has been proposed as a complementary instrument for contour measurement and verification. This is mostly due to the relative insensitivity of the CD-AFM to material properties, the three-dimensional nature of the data, and the ability to make the instrument traceable to the *SI* unit of length. Although data from CD-AFM is inherently three dimensional, the planar two-dimensional data required for contour metrology is not easily extracted from the top-down CD-AFM data. This is largely due to the limitations of the CD-AFM method for controlling the tip position and scanning. In this paper, we outline a method for acquiring contour data using the CD-AFM. The paper is organized as follows; in Sec. 2 we describe how the CD-AFM measures contours, including image acquisition and contour extraction. In Sec. 3 we examine the uncertainty associated with drift correction, followed by comparisons with SEM and helium ion microscope (HIM) images in Sec. 4. The work concludes with a summary in Sec. 5.

2.   CD-AFM CONTOUR MEASUREMENT

2.1   Image Acquisition

In measuring contours with the CD-AFM, a key goal is to make sure the advantages of the CD-AFM highlighted above are maintained. One of the conclusions of our previous report [8] was that to capture top down images of features in two directions, at least two measurements in different axes will be needed. This is necessitated by the way the CD-AFM acquires data. Tip – sample interaction information is obtained in one direction and the scan lines are assembled together to form a three dimensional image. For a particular measurement, width information is only in one direction, even though the height map is three dimensional. In the images of figure 1, only sidewall information along features perpendicular to the scan axis is captured. So, based on the current operation of the CD-AFM (and other AFMs), to obtain a full contour representation involving sidewall information is not possible with one image.
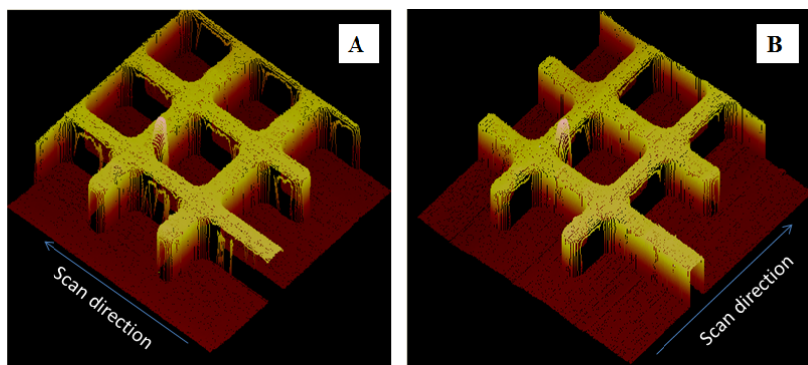

Figure 1: CD-AFM images of the same feature taken at different scan directions. (A) The image was acquired with the cantilever scanning along the x-axis. (B) Image acquired with the cantilever scanning along the y-axis. Note the complementary regions of missing data in both images.

Our solution is to extract contour information from the two images. This provides sidewall data that could be used to form an accurate two dimensional top-down contour profile. Our solution is to acquire images in two orthogonal directions. This provides sidewall data that could be used to form an accurate two dimensional top-down contour profile. The actual data acquisition is relatively straight forward, the key is to find a way to extract and combine profiles from the two images while keeping the uncertainty within a reasonable range. In acquiring the images, the sample or the scan direction could be rotated. Changing the tip scan direction ensures that the sample is not moved, and any drift due to the sample stage will be the same in both images. However, the tip in some systems is mounted at an angle in one scan direction. In this case, rotating the sample will be a better trade-off. In both cases, the uncertainty implications (discussed below) should be accounted for. Extracting contours from the two images is discussed in the next section.

2.2   Contour Extraction

The main objective here is to extract contours from the two images, and combine them in such a way that the width information from both axes is consistent. To do this, we make use of various locations that are present in both images.

These include some of the corners, rounded edges, and all of the height information. A closer look at the images in figure 1 shows the CD-AFM was able to acquire some data at the edge of the sample. Usually, the data from this location is sparse, but enough for our purposes. These locations, which we call critical points, act as registration markers for combining the profiles. The procedure for obtaining the contour profiles is outlined in figure 2 and works as follows. The first step is to identify the scan lines from the overlapping section of the two images, and calculate the heights, and sidewall angles. The second step we match the profiles from the two orthogonal scans. Since the profiles are not in the same direction, a perfect match is not the objective; rather we need to have enough confidence to identify areas where extracted profiles can overlap. An optional step is to take the cross-correlation function of the two profiles (or portions) and see if it is a good match. Figure 3 shows two overlaid profiles from the same corner taken from different scan directions. Because of variability in tip positioning, there is no guaranty overlapping profiles are from the exact same location.

Calculate parameters for the two images - { height, width, sidewall angle}

Identify and match critical points

Calculate cross correlation if needed
$$\left| (r * \rho)\tau = \sum_{\infty} r(x)\rho(x+\tau)dx \right|$$

Determine height level for line extraction

Extract Contours

Check height value with SEM data

no

Yes

Combine profiles

Develop uncertainty estimate $u_c^2(y) = \sum_{i=1}^{N}\left(\frac{\partial f}{\partial x_1}\right)^2 u^2(x_i) + 2\sum_{i=1}^{N-1}\sum_{j=i+1}^{N}\frac{\partial f}{\partial x_i}\frac{\partial f}{\partial y_j}u(x_i, x_j)$
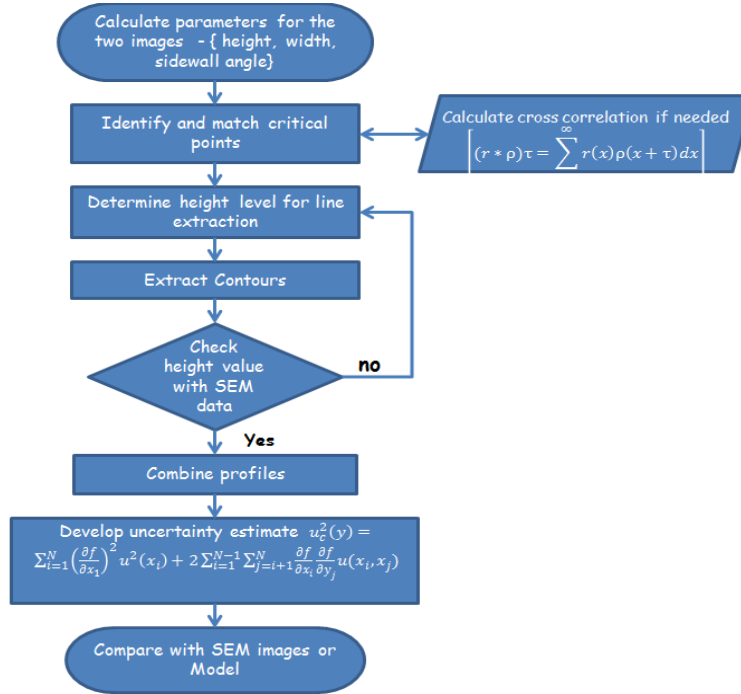
Compare with SEM images or Model

Figure 2: Flow chart of the contour determination and matching process
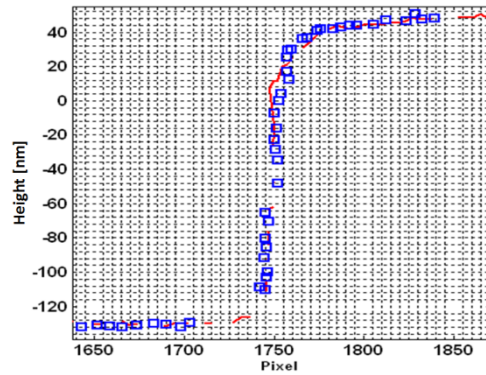
Figure 3: Profiles from one of the critical points taken from two different directions.

The third step is to extract the contours from a predetermined height location. Since some (or most) of the features will not have a 90 degree sidewall, care should be taken to ensure the height level used makes sense for the application. For example, if the final contour profiles will be compared with SEM contours, then height location of AFM contours should be consistent with the SEM edge determination algorithm used. In the contour extraction procedure, this is checked by comparing the contours with SEM images. This ensures changes are made now rather than at the end. We assume SEM information will be known *a priori*. The next step is to fit the lines. As shown in subsequent figures, this has the effect of smoothing the lines. Using the fitted lines for the final SEM comparison ensures clean "overlay" of the profiles, but has the effect of removing line edge roughness. There is also some uncertainty associated with the goodness of fit, and combining different fitted lines. The extracted contours from both images are then combined, followed by an estimate of the uncertainty budget. The profiles are then compared with SEM images. Figure 4 shows extracted edge profiles from one scan direction. Figure 5 shows a combined plot of full profile obtained from two CD-AM images. For features like the one shown in figure 1, an edge definition algorithm could be used to define the edges, and calculate the center point of the grid which could then be used to align the extracted contours.

The main limitations of the technique include increased measurement time, and unstable tip sample interaction at the inner corners. The current work uses a series of scanning and analysis techniques to work around some of AFM limitations, but does not actually correct those limitations.
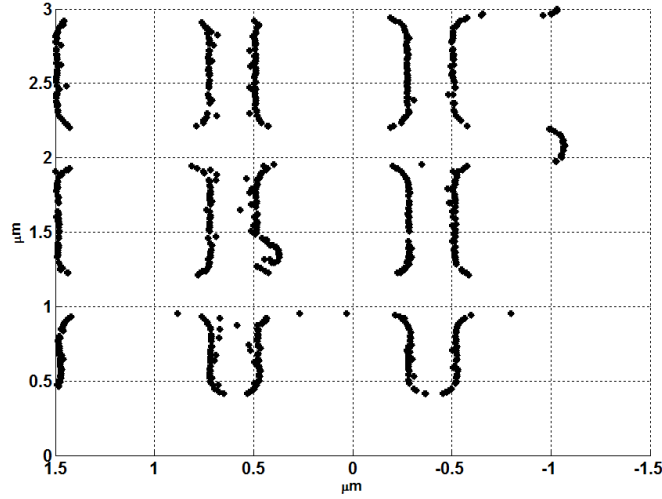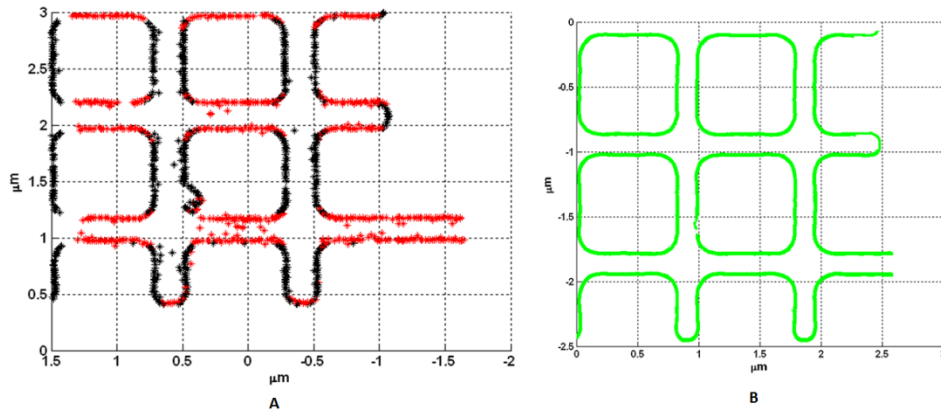

Figure 4: Extracted edge profiles (contours)

Figure 5: (A) Raw contours for the grid sample in two directions. (B) Fitted lines from the contours. The tip width is accounted for in the fitted lines.

3. UNCERTAINTY COMPONENTS

In addition to uncertainty components one would normally see in a CD-AFM [9-15], there are a few others that could be introduced by the methods described above. These could include drift, tip size limitations, tip/sample interaction, sample rotation errors, and uncertainty of the line fits [8]. Here we go into detail and describe the stage drift information into the uncertainty. One way to account for the stage drift is to consider the tip and the sample stage as independent axes represented by equations 1 and 2.

$$ {}^{t}\vec{X}_{t} = \begin{bmatrix} {}^{t}x_{t} \\ {}^{t}y_{t} \\ 1 \end{bmatrix} \tag{1} $$

$$ {}^{s}\vec{X}_{s} = \begin{bmatrix} {}^{s}x_{s} \\ {}^{s}y_{s} \\ 1 \end{bmatrix} \tag{2} $$

In these equations: s stands for the sample stage. A value of 1 indicates we are not considering drift in the z axis. The question of whether to consider drift in z will depend on the application and system. In some systems, the x-y drift could be induced by settling in the z axis. Although the absolute z level of the stage may be drifting, this may not be reflected in the feature height being measured. Ideally, during measurement equation 1 equal to equation 2. This represents the condition when the tip first engages. A schematic diagram of the two coordinate systems is shown in figure 6.
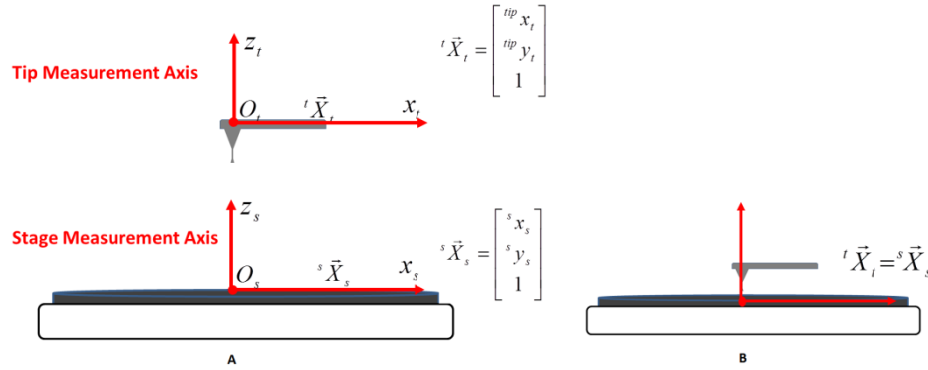

Figure 6: (A) Schematic diagram of the tip and stage coordinate systems, (B) Schematic diagram of tip and stage measurement systems during initial engage

As the sample stage starts to drift, instead of equation 1 being equal to equation 2, one gets equation 3. If the tip is used as the reference axis, then the resulting motion could be represented as the motion of the stage plus any additional displacements.

$$\mathrm{^{tip}\vec{X}_t = {}^s\vec{X}_s + \begin{bmatrix} \delta_x \\ \delta_y \\ \delta_z \end{bmatrix}} \tag{3}$$

As above, δ_x, δ_y, and δ_z are drift in the x, y, and z axes. The homogeneous matrix of the above procedure could be represented as

$$\begin{bmatrix} \overset{P'}{{}^{tip}\vec{X}_t} \\ {}^{tip}\vec{Y}_t \\ 1 \end{bmatrix} = \overset{T(\delta_x, \delta_y)}{\begin{bmatrix} 1 & 0 & \delta_x \\ 0 & 1 & \delta_y \\ 0 & 0 & 1 \end{bmatrix}} \begin{bmatrix} \overset{P}{{}^s x_s} \\ {}^s y_s \\ 1 \end{bmatrix} \tag{4}$$

$$P' = T(\delta_x, \delta_y)P \tag{5}$$

It is important to point out that we did not consider rotation. The stage is constrained in the rotational direction. Also δ_x and δ_y are the actual drift when the stage is supposed to be steady, rather than additional displacements when the stage is in motion. These values are treated as offsets and used to correct for drift. To obtain an uncertainty value after correction, multiple drift measurements are taken and averaged. We assumed a rectangular distribution, with the peak-to-valley value of the residuals used as the bounds of the interval. This does not give the uncertainty of the drift, rather the uncertainty of the drift correction. Justification for this type of treatment is based on the drift being determined *a priori* and corrected. For this type of distribution the lower and upper limits of a_- and a_+ means we are sure the uncertainty values are within this interval. In our case, this only works if we use the maximum drift (rather than the average drift) of the system as δ_x and δ_y values. This is a rather conservative estimate because the rectangular probability distribution assumes that the uncertainty value could lie anywhere within the specified interval. For our purposes it ensures we do not underestimate the drift correction uncertainty component. This results in an uncertainty value of $u_{drift\ Correction} = a/\sqrt{3}$, where a is the peak-to-valley value of the drift residuals. The combined uncertainty expression (equation 6) comes from a Taylor series expansion of the estimate ($Y = f(X1, X2, ... X_N)$) of the individual uncertainty components ($[(x_1, u_1), ... (x_m, u_m)]$) listed above.

$$u_c^2(y) = \sum_{i=1}^{N} \left(\frac{\partial f}{\partial x_1}\right)^2 u^2(x_i) + 2\sum_{i=1}^{N-1} \sum_{j=i+1}^{N} \frac{\partial f}{\partial x_i} \frac{\partial f}{\partial y_j} u(x_i, x_j) \tag{6}$$

$u(x_i, x_j)$ is the estimate of the covariance and goes to zero if the components are not correlated. The total uncertainty of the profiles shown in figure 5B is 1.8 nm (k=1). This comes mostly from the inner corners, which had higher uncertainty values than the rest of the image.

Preprint

4. COMPARISON WITH SEM AND HIM

The objective of extracting contours is to compare the information with those obtained from another instrument, model, graphic database system files (GDSII), or all of the above. We compared the extracted contours with those from both the SEM and the HIM. Care should taken to ensure AFM data is extracted from height levels that are consistent with the algorithm used for SEM and HIM edge determination, or else differences in size could be confused with scale offsets. Figure 7A shows an SEM image of the feature in figure 1, and figure 7b shows the extracted profiles in figure 5B overlaid with the SEM edge positions. Corresponding images for the HIM are shown on figure 8. Figure 9 A shows, extracted profiles from the CD-AFM, the fitted lines are shown on figure 9B. Figure 10 shows SEM and HIM images of the same feature in figure 9, and the overlaid AFM contours. In terms of the overall shape, the profiles are a good match. We have not yet developed a metric to quantify how well the contours match. In their SEM work, Hibino et al. [1] uses a metric called $Contour_{RMS}$ to quantify the mismatch between measured and simulated contours. We are exploring if such a metric would be suitable for our use.
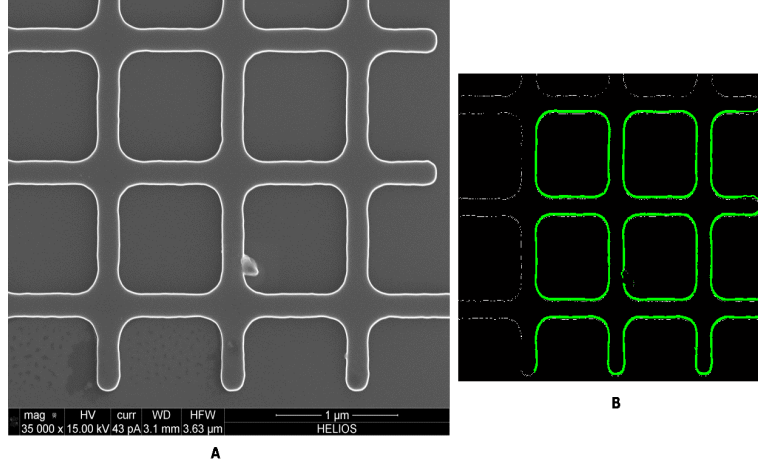

Figure 7: (A) SEM images of a test sample (B) Contours extracted from the SEM images overlaid with contours extracted from two CD-AFM images.
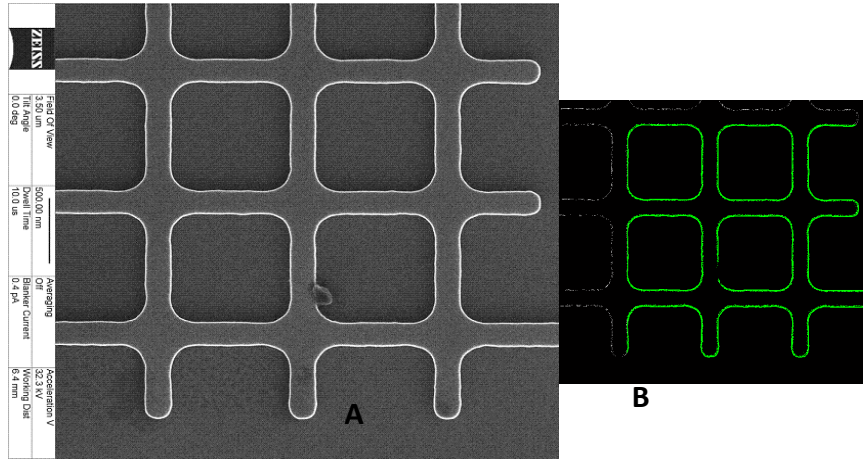

Figure 8: (A) HIM images of a test sample (B) Contours extracted from the SEM images overlaid with contours extracted from two CD-AFM images.
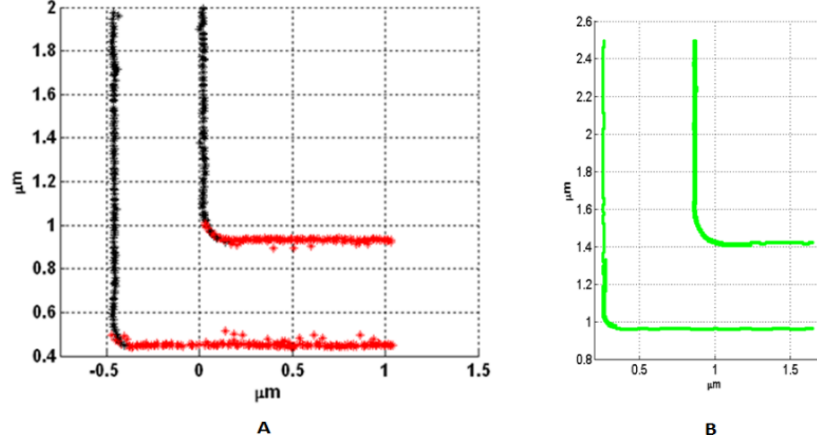
Figure 9: (A) Raw contours extracted from CD-AFM images to form a composite contour profile. (B) Fits extracted from the profile in (A). The tip width is accounted for in the fitted lines.
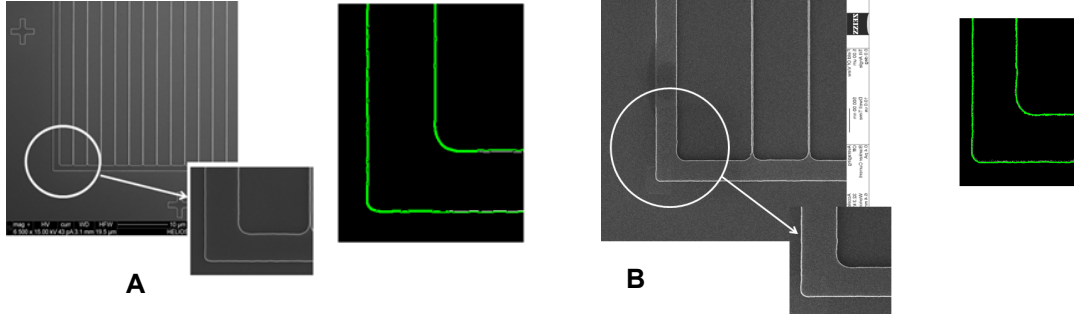

Figure 10: (A) SEM images of a test sample and contours extracted from the SEM images overlaid with contours extracted from two CD-AFM images. (B) HIM images of a test sample and contours extracted from the HIM images overlaid with contours extracted from two CD-AFM images.

5. SUMMARY AND CONCLUSIONS

In this paper, we outlined measurement and analysis techniques to extract contours from CD-AFM images. The technique requires the use of two images taken from orthogonal scan directions, and combing contours extracted from those images. We also listed some of the uncertainty components associated with our techniques, and presented an in-depth treatment of the drift correction uncertainty. Some limitations of our technique include the increased overhead of acquiring and analyzing two images, and carefully accounting for the additional uncertainty sources. Overall, our work shows that two down contours can be reliably extracted from CD-AFM images with a standard uncertainty ($k = 1$) of 1.8 nm.

Future work include developing a metric to quantify the mismatch between AFM contours and those extracted from other techniques, and comparing the data with the GDSII file information, completing work on real time stage drift monitoring.

Preprint

6. REFERENCES

[1] D. Hibino, H. Shindo, Y. Abe, Y. Hojyo, G. Fenger, T. Do, I. Kusnadi, J. L. Sturtevant, J.Van de Kerkhove, P. De Bisschop, "High-accuracy optical proximity correction modeling using advanced critical dimension scanning electron microscope–based contours in next-generation lithography," *J. Micro/Nanolith. MEMS MOEMS* 10(1), 013012 (2011)

[2] L. Zhu, X. Kang, Y. Gu, S. Yang, "Study of the contour-based optical proximity correction methodology," *J. Micro/Nanolith. MEMS MOEMS* 8(4), 043005 (2009)

[3] U. Klostermann, T.Mülders, D. Ponomarenco, T .Schmöller, J. Van de Kerkhove, P. De Bisschop, "Calibration of physical resist models: methods, usability, and predictive power," *J. Micro/Nanolith. MEMS MOEMS* 8(3), 033005 (2009)

[4] P. De Bisschop, J. Van de Kerkhove, "Alignment and averaging of scanning electron microscope image contours for optical proximity correction modeling purposes," *J. Micro/Nanolith. MEMS MOEMS* 9(4), 041302 (2010)

[5] Yeon-Ah Shim, J. Kang,S-U Lee,J. Kim, and K. Kim, "Methodology to set-up accurate OPC model using optical CD metrology and atomic force microscopy," *Proc. SPIE* 6518, 65180C (2007); doi: 10.1117/12.711936

[6] V. A. Ukraintsev, "Role of CDAFM in achieving accurate OPC modeling," *Proc. SPIE* 7272, 727205 (2009); doi: 10.1117/12.815240

[7] J.S. Villarrubia, R.G. Dixson, and A.E. Vladár "Proximity-associated errors in contour metrology" Proc. SPIE 7638, 76380S (2010); doi: 10.1117/12.848406

[8] N.G. Orji, R.G. Dixson, A.E. Vládar, and M.T. Postek ″Strategies for nanoscale contour metrology using critical dimension atomic force microscopy″ *Proc. SPIE* 8105, 810505 (2011); doi: 10.1117/12.894416

[9] R. G. Dixson, R. A. Allen, W. F. Guthrie, and M. W. Cresswell, "Traceable calibration of critical-dimension atomic force microscope linewidth measurements with nanometer uncertainty," *J. Vac. Sci. Technol B* Vol. 23, 3028-3032 (2005)

[10]   R. Dixson, J. Fu, N.Orji, W. Guthrie, R. Allen and M. Cresswell, "CD-AFM reference metrology at NIST and SEMATECH", *Proc. SPIE 5752, 324* (2005); doi: 10.1117/12.601972

[11]   N. G. Orji; R. G. Dixson; D.I. Garcia-Gutierrez; B. D. Bunday, M. Bishop, M. W. Cresswell, R. A. Allen, J. A. Allgair, "TEM calibration methods for critical dimension standards," Proc. SPIE 6518, 651810 (2007); doi: 10.1117/12.713368

[12]   N G Orji and R G Dixson, "Higher order tip effects in traceable CD-AFM-based linewidth measurements," Meas. Sci. Technol. 18 448 (2007)

[13]   N.G. Orji, R. G. Dixson, A. Martinez, B.D. Bunday, J.A Allgair, T. V. Vorburger, "Progress on Implementation of a CD-AFM-Based Reference Measurement System," J. Micro/Nanolith. MEMS MOEMS 023002-9 6(2) (2007)

[14]   N.G. Orji,, R.G. Dixson, A.M. Cordes, B.D. Bunday, and J.A. Allgair, "Measurement traceability and quality assurance in a nanomanufacturing environment," J. Micro/Nanolith. MEMS MOEMS 10, 013006 (2011)

[15]   R. Dixson, N.G. Orji, C.D. McGray, J. Bonevich, J.Geist, "Traceable calibration of a critical dimension atomic force microscope" J. Micro/Nanolith. MEMS MOEMS 11, 011006 (2012)